Journal of Thermal Analysis and Calorimetry, Vol. 88 (2007) 1, 237–243

THERMAL STABILITY AND SINTERING BEHAVIOUR OF HYDROXYAPATITE NANOPOWDERS

Alessandra Bianco[1*], *Ilaria Cacciotti*[1], *Mariangela Lombardi*[2], *Laura Montanaro*[2] *and G. Gusmano*[1]

[1]University of Rome Tor Vergata, Dept. of Chemical Sciences and Technologies, INSTM Research Unit Tor Vergata, Via della Ricerca Scientifica 1, 00133 Roma, Italy
[2]Politecnico of Torino, Dept. of Materials Science and Chemical Engineering, INSTM Research Unit Politecnico di Torino: LINCE Lab, Corso Duca degli Abruzzi 24, 10129 Torino, Italy

Hydroxyapatite (HA) nanopowders were synthesised following two different precipitation routes: (a) from calcium nitrate and diammonium hydrogen phosphate solutions and (b) from calcium hydroxide suspension and phosphoric acid solution. The influence of precipitation process, concentration, and synthesis temperature on HA particle size and morphology, phase composition, thermal stability, and sintering behaviour was investigated by means of: thermogravimetry and differential thermal analysis (TG-DTA), induced coupled plasma–atomic emission spectroscopy (ICP-AES), Fourier transform infrared spectroscopy (FTIR), X-ray diffraction (XRD), electron microscopy (TEM, SEM) and dilatometry.

Keywords: *hydroxyapatite, nanopowders, sintering, thermal stability*

Introduction

The role of hydroxyapatite ($Ca_{10}(PO_4)_6(OH)_2$, HA) in biomedical application, such as synthetic bone grafts and scaffolds for hard tissue engineering is well known. Various synthesis procedures [1–6] have been explored to produce nano-sized HA, since they exhibit improved bioactivity with respect to coarse powders [7]. In addition, HA nano-particles can be blended into bioresorbable polymers to realise composites with superior mechanical properties [8].

Literature has largely demonstrated that the synthesis routes and related parameters could significantly affect not only HA particle size and morphology, but also phase composition, thermal stability as well as sintering behaviour [9–18]. However, recently, there has been an evident lack of publications reporting systematic studies dealing with the effect of synthesis parameters (reaction temperature, pH, nature and concentration of the reactants) on resulting HA powders [8]. Moreover, limited data on nanopowders are available [1, 19–21].

In this paper, the influence of precipitation route and main process parameters (synthesis temperature, nature and concentration of reagents) on thermal stability and densification behaviour of nano-sized HA powders is reported.

Experimental

Materials

Nano-sized HA powders were prepared in a double-walled jacket reactor (to control synthesis temperature) under magnetic stirring (around 400 rpm) following two different precipitation routes:

- from calcium nitrate
- from calcium hydroxide

Stoichiometric volume of calcium nitrate tetrahydrate ($Ca(NO_3)_2{\cdot}4H_2O$, Aldrich 99.2%) aqueous solution was added dropwise to diammonium hydrogen phosphate ($(NH_4)_2HPO_4$, Aldrich 99.2%) aqueous solution. As resumed in Table 1 different ex-

Table 1 Powder designation and process parameters

Powder	Reactant	*T*/°C	Precipitation pH (*final pH)	$[Ca^{2+}]$/mol L^{-1}
HAN1	calcium nitrate	40	10.0	1.0
HAN2	calcium nitrate	70	10.0	1.0
HAN3	calcium nitrate	40	10.0	0.5
HAI1	calcium hydroxide	40	9.4*	1.0

* Author for correspondence: bianco@stc.uniroma2.it

1388–6150/$20.00

Akadémiai Kiadó, Budapest, Hungary
Springer, Dordrecht, The Netherlands

perimental conditions were considered. The following reaction occurred:

$$10Ca(NO_3)_2+6(NH_4)_2HPO_4+2H_2O\rightarrow Ca_{10}(PO_4)_6(OH)_2+12NH_4NO_3+8HNO_3$$

During precipitation, the pH was continuously monitored and adjusted at 10±0.1 by adding NH_4OH conc. Precipitates were aged in mother liquor for 24 h at room temperature and then washed several times with NH_4OH aqueous solution (pH 10). As-precipited products were vacuum filtered and finally dried in oven at 60°C for a few hours.

An aqueous suspension of calcium hydroxide ($Ca(OH)_2$, Aldrich 99.5%) was titrated with phosphoric acid (H_3PO_4, Aldrich 86.3%). The following reaction occurred:

$$10Ca(OH)_2+6H_3PO_4\rightarrow Ca_{10}(PO_4)_6(OH)_2+18H_2O$$

The pH was finally adjusted at 9.4. As-precipitated powder was aged in mother liquor for 24 h at room temperature and washed several times with NH_4OH aqueous solution (pH 9.4). The product was vacuum filtered and finally dried in oven at 60°C for a few hours.

In both cases, dried powders were wet milled in a planetary mill for 1 h in absolute ethanol, by using agate grinding media.

In order to compare synthesised powders, precipitation route and selected process parameters (calcium ion concentration and precipitation temperature) have been changed one by one.

Methods

Chemical analyses of either as-precipitated powders and mother solutions were performed by induced coupled plasma atomic emission spectroscopy (AES-ICP, JobinYvon JV 24R).

The thermal behaviour of as-precipitated samples was investigated by simultaneous thermogravimetry and differential thermal analysis (TG-DTA, Netzsch STA 409; sample mass: about 60 mg; heating rate: 10°C min^{-1}; maximum temperature: 1250°C; air flow: 80 cm^3 min^{-1}). On the grounds of these observations, a thermal pre-treatment of as-precipitated powders before sintering was stated. It must be noted that the sintering behaviour of HA is strongly affected by calcination [10, 17].

Microstructural features of as-precipitated powders were studied by transmission electron microscopy (TEM, Philips CM120; bright field mode; accelerating voltage:100 kV).

Infrared spectra (Fourier transform infrared spectroscopy, FT-IR 16 F PC Perkin Elmer) were recorder between 500 and 4000 cm^{-1} using KBr pellets (1 mass/mass%), the spectral resolution being 4 cm^{-1}.

Phase evolution with temperature was followed by X-ray diffraction (XRD, Philips 1710; CuK_α radiation, investigated range: 20–55° 2θ) on powdered samples calcined at different temperatures in the range 600–1400°C for 1 h.

The crystallinity degree (X_c), corresponding to the fraction of crystalline phase present in the examined volume, was evaluated as follows:

$$X_c\approx 1-(V_{112/300}/I_{300})$$

where I_{300} is the intensity of (300) reflection of HA and $V_{112/300}$ is the intensity of the hollow between (112) and (300) reflections, which completely disappears in non-crystalline samples. In agreement with Landi *et al.* [13] a verification was done as follows:

$$B_{002}\sqrt[3]{X_c}=K$$

where K is a constant found equal to 0.24 for a very large number of different HA powders, and B_{002} is the full width at half maximum (in degrees) of reflection (002).

Before sintering, as-precipited powders were calcinated at 600°C for 1. The particle size distribution of aggregates was determined by means of a laser diffraction particle analyzer (Fritsch, Analysette 22 Compact). For this purpose, samples were suspended in ethanol and then sonicated.

Sintering was performed on bars obtained by uniaxially pressing (400 MPa) HA powders pre-treated at 600°C for 1 h. The sintering behaviour was followed by dilatometry (Netzsch 402E, heating and cooling rate: 10°C min^{-1}; maximum temperature: 1250°C; soaking time at the maximum temperature: 1 h; static air). On the grounds of the derivative curves, the maximum densification temperature was determined. Futher, HA green bodies, obtained by uniaxially pressing the nanopowders at 400 MPa, were sintered up to the chosen temperature in a programmed furnace.

Density was evaluated by geometrical and mass measurements. Powders pre-treated at 600°C and fracture surfaces of sintered bodies were observed by scanning electron microscopy (SEM, Hitachi S2300).

Results and discussion

ICP-AES results on as-precipitated powders and mother solutions are reported in Tables 2 and 3 respectively.

The synthesis from $Ca(NO_3)_2\cdot 4H_2O$ allowed a very strict control of the precipitate composition. In fact, the Ca/P molar ratio of HAN powders is very

Table 2 ICP-AES analysis of as-precipitated powders

Powder	Ca/P molar ratio	Mg mol% *vs.* Ca	Sr mol% *vs.* Ca
HAN1	1.6585	0.076	0.008576
HAN2	1.6694	0.083	0.008597
HAN3	1.6652	0.120	0.009440
HAI1	1.7034	0.778	0.020100

Table 3 ICP-AES analysis of mother solutions

Mother solutions	Ca/mmol L^{-1}	P/mmol L^{-1}
HAN1	0.490	$<10^{-2}$
HAN2	0.125	$<10^{-2}$
HAN3	1.297	1.215
HAI1	0.051	4.610

close to the stoichiometric value 1.667. In the final powders, tiny amounts of Sr and Mg, both diadochic of Ca^{2+} in the HA lattice, present as impurities in the reactants, were detected [22, 23]. In all cases only slight amounts of un-reacted Ca and P were detected by ICP-AES in mother solutions, reaction yields being thus nearly quantitative. Moreover, the trend is in very good agreement with Ca/P molar ratio of HA powders.

In the case of the synthesis from $Ca(OH)_2$ a strong deviation (about 2.2%) from the ideal Ca/P molar ratio was observed, clearly due to a more relevant loss of P in the mother solution. Contamination from Mg and Sr is also higher due to the lower purity of raw materials. The effect of deviation from stoichiometry and impurity content on thermal stability of HAI product will be described in the following paragraphs.

XRD patterns of the four as-dried powders are collected in Fig. 1. In all samples, only HA reflections were detected. The crystallinity degree ranged between 20 and 25% for HAN1 and HAN3 synthesised at 40°C, whereas it is augmented up to about 45% for

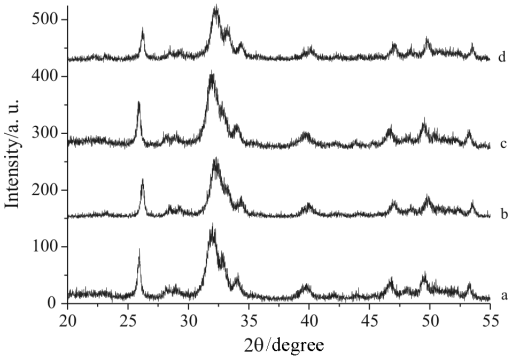

Fig. 1 XRD patterns of as-precipited powders: a – HAN1; b – HAN2; c – HAN3; d – HAI1

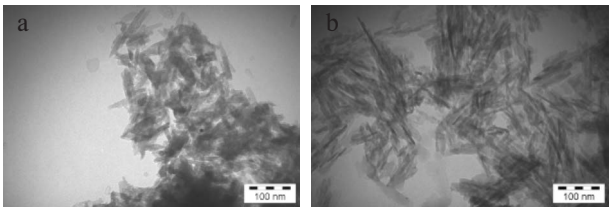

Fig. 2 TEM images (175.000x) of as-precipited powders: a – HAN1; b – HAN2

HAN2 prepared at 70°C. The increase of crystallization degree by increasing precipitation temperature is a well known phenomenon in the wet syntheses of HA and many other oxides [13, 24, 25]. A similar pattern was also recorded for HAI1, whose crystallization degree is about 25%.

TEM observations (Figs 2a and b) revealed that all the precipitated powders are made of nano-sized, needle-like particles of about 10–20 nm in width and 50–200 nm in length. The shape factor (about 3–5) of materials synthesised at lower temperature was smaller, independently from the other synthesis parameters (Fig. 2a). In the case of sample HAN2 prepared at 70°C, it increases up to about 10 (Fig. 2b). This effect of synthesis temperature on powders morphological features is in agreement with the studies of Pang *et al.* [26] and Bouyere *et al.* [27].

TG curves of the four powders are reported in Fig. 3. In order to avoid the large effect due to the evaporation of adsorbed water, the temperature range 150–1000°C was considered. For all samples, the mass loss between 150 and 600°C ranges within 3 and 5%. According to other authors [26, 28], it is probably associated to the elimination of carbonates and combined water. DTA curves show a broad and weak peak, associated to this mass loss. Above 600°C no other losses were detected. On the grounds of thermal analyses and previous literature statements [10, 12, 13, 17], as-precipitated powders were pretreated at 600°C for 1 h prior sintering.

The thermal stability of HA nanopowders was investigated by FTIR and XRD analyses performed

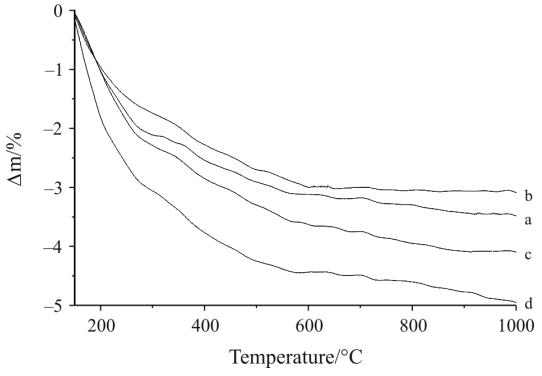

Fig. 3 TG curves of as-precipited powders from 150 to 1000°C: a – HAN1; b – HAN2; c – HAN3; d – HAI1

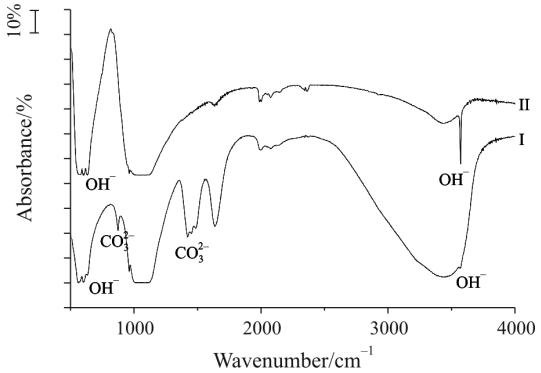

Fig. 4 FTIR spectra of HAN2: I – as-precipited; II – after calcination at 1100°C

either on as-precipitated powders and on powders calcined at different temperatures.

FTIR spectra of the four powders are quite similar. As an example, the spectrum of HAN2 either as-precipited and calcined (1100°C, 2 h) are compared in Fig. 4.

As-precipited samples show the characteristic pattern of hydrated partially carbonated hydroxyapatite [26–29]: ν_{OH} (3570 cm^{-1}) and δ_{OH} (633 cm^{-1}); $\nu_{1(PO_4)}$ (962 cm^{-1}), $\nu_{3(PO_4)}$ (broad band 1040–1090 cm^{-1}) and $\nu_{4(PO_4)}$ (565 and 603 cm^{-1}); $\nu_{2(CO_3)}$ (875 cm^{-1}) and $\nu_{3(CO_3)}$ (1420 and 1457 cm^{-1}). The broad band at 2500-3700 cm^{-1} and the sharp peak at 1637 cm^{-1} have to be associated to the presence of either absorbed and combined water. The lack of the characteristic $\nu_{3(CO_3)}$ peak at 1550 cm^{-1}, suggests that only B-type carbonated hydroxyapatite is formed.

Besides, the shoulder at about 1490 cm^{-1} has also to be considered. It is reported that this band can be assigned either to a carbonate ion in a second unspecified location [30], to a second B-type carbonate [31], or to a carbonate ion in an amorphous carbonated hydroxyapatite phase [32, 33]. According to literature, the presence of carbonate ion within the as-precipited apatite phase inhibits significantly the conversion of the amorphous to the crystalline phase [32, 34], being thus responsible for the low crystallinity of as-precipited samples as evidenced by XRD results. In all cases the characteristic peaks (540–530, 855, 1130 and 1210 cm^{-1}) of HPO_4 were not detected [28]. Moreover, the lack of bands in the range 700–750 cm^{-1} indicates the absence of calcium carbonates, i.e. calcite (712 cm^{-1}), aragonite (713 and 700 cm^{-1}) and valerite (745 cm^{-1}). Finally, the absorption band at 1385 cm^{-1} ascribed to nitrate is also absent, suggesting that washings were efficient. In conclusion, FTIR analysis shows that as-precipited powders consist of hydrated partially carbonated hydroxyapatite, the carbonate groups substituting the phosphate groups in the HA lattice and within the amorphous phase.

FTIR spectra of calcined samples differ considerably from those of as-precipited materials. In details, all CO_3 bands disappear, the intensity of peaks associated to H_2O is remarkably decreased, the intensities of OH vibration modes increase remarkably. The persistence of OH groups suggests that, up to 1100°C, the dehydroxylation of hydroxyapatite did not occur. In conclusion, according to these results, the thermal treatment of as-precipited powders induces elimination of carbonates and combined water, without any detectable further decomposition.

XRD patterns of the four powders calcined at different temperatures within the range 600–1400°C (soaking time 1 h) are collected in Figs 5a–d.

At 600°C a poorly crystallized HA is present in all investigated materials. The deviation of Ca/P molar ratio in HAI1 does not affect phase stability. On the contrary, this powder retains the HA phase up to 1400°C, whereas the three HAN powders present firstly the appearance of β-TCP, above 800°C, and then variable amounts of α-TCP, starting from 1200°C.

Dehydroxylation of HA was observed starting from 1400°C just in the case of HAI1, as revealed by the peaks shifted by about 0.1°of 2θ (see the insert in Fig. 5d), indicating that the HA lattice had contracted due to OH loss [35].

The morphology of powders calcined at 600°C was investigated by SEM (Figs 6a and b), particle size distributions being compared in Fig. 7. HAN1 and HAN3 presented a very similar, monomodal particle size distribution centred around a mean value of about 3.5 microns, according to SEM images (Fig. 6a). Powders HAI1 showed a slightly broader distribution with a mean size of about 5 microns. Finally, powder HAN2 is characterised by an almost bimodal distribution and by the presence of large agglomerates, as confirmed by SEM observations (Fig. 6b). Therefore, the powder HAN2 synthesized at higher temperature (70°C) is more agglomerated, in excellent agreement with the agglomeration behaviour of HA precipitated from calcium hydroxide at 35 and 70°C, respectively [13].

The dilatometric behaviour of the four powder compacts up to 1250°C is reported in Fig. 8. The starting and final densities (referred to the theoretical value of pure HA, 3.08 g cm^{-3}), the total linear shrinkage and the inflection point (temperature of the peak on the derivative curve corresponding to the maximum densification rate) are collected in Table 4.

All the powders presented an inflection point at about 1030±20°C, in good agreement with the maximum densification temperature of nanosized HA powders [19, 36] and of powders pre-treated prior sintering at low temperatures [10]. The highest shrinkage was recorded for HAN3. However, the

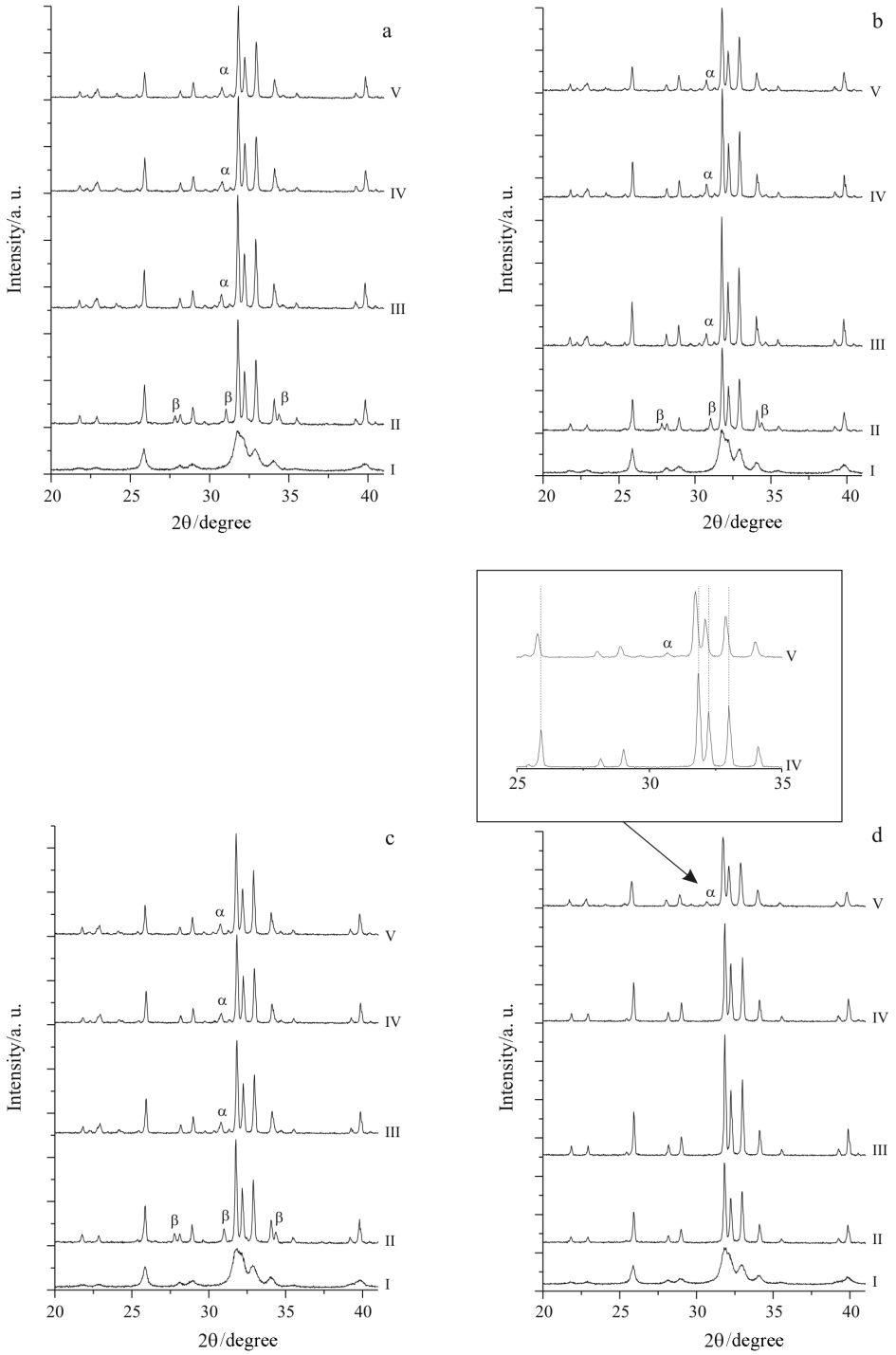

Fig. 5 XRD patterns of powders calcined at different temperatures for 1 h: I – at 600; II – at 1100; III – at 1200; IV – at 1300; V – at 1400°C; a – HAN1; b – HAN2; c – HAN3; d – HAI1 (in the insert, detail of the peaks shift)

most relevant difference in shrinkage and final density was observed in sample HAN2, the latter achieving a slightly lower final density. This result has to be attributed to the difference in green density induced by the presence of larger agglomerates and subsequent lower packing efficiency.

In the case HAN samples, it has to be considered that an under-estimation of the final density values as a percentage of d_{th} is expected since sintered materials contain a certain amount of α-TCP whose theoretical density (2.81 g cm^{-3}) is lower with respect to the theoretical density value of HA (3.08 g cm^{-3}). On the contrary, sintered HAI1 samples display only the HA phase, so that the reference to the theoretical density value of HA (3.08 g cm^{-3}) is consistent for sintered bodies.

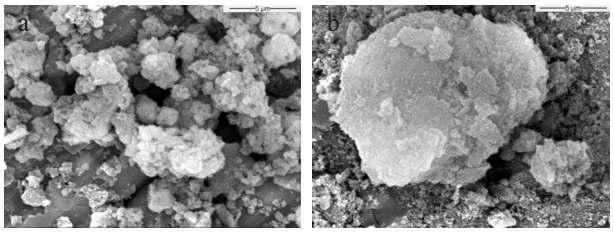

Fig. 6 SEM images (5000x) of powders pre–treated at 600°C for 1 h: a – HAN1; b – HAN2

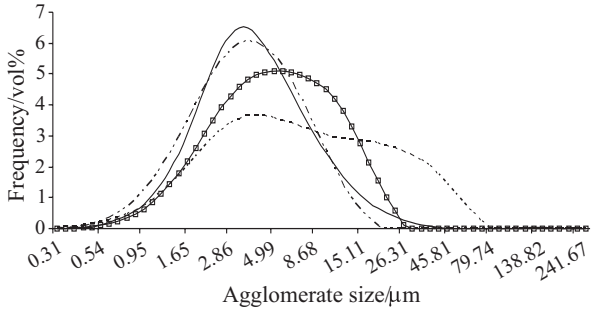

Fig. 7 Particle size distribution of the powders pre–treated at 600°C for 1 h: — HAN1; · · · HAN2; – · · – HAN3; squares HAI1

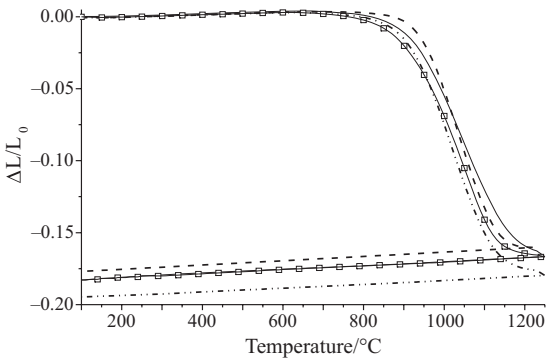

Fig. 8 Dilatometric curves of the four HA powders: — HAN1; – – – HAN2; – · · – HAN3; squares HAI1

In order to investigate the influence of the upper sintering temperature on density and final microstructure, pellets were sintered at 1050°C for 3 h, fired densities are reported in Table 4. It has to be pointed out that all sintered HAN materials showed β-TCP (theoretical density 3.12 g cm^{-3}) as second phase.

The final density of HAI1 samples sintered at 1050°C was not significantly different from that recorded for samples sintered at higher temperature. In the case of HAN materials, a more or less evident decrease in densification was observed.

The microstructure of materials sintered at 1050 or at 1250°C are compared in Fig. 9.

After sintering at 1250°C a relevant grain growth and coalescence are observed, mostly in the case of HAN1 and HAI1, whose microstructures appear as a continuous media with residual porosities mainly at the triple joints (Fig. 9a). Grain coalescence is less evident in the case of HAN2 and HAN3, even if grain growth is still relevant (Fig. 9b). After densification at 1050°C, HAI1 presented a fine and homogeneous microstructure, made of both nanometric grains and pores (Fig. 9c). On the contrary, the three HAN materials presented a more significant grain growth and dishomogeneous microstructure, more evident in the case of HAN2 (Fig. 9d). This difference in microstructure could be attributed to the strength of agglomerates. Precipitation from Ca hydroxide produces probably softer agglomerates that are almost completely crushed under the uniaxial pressure applied to prepare green bodies. On the contrary, it seems that the precipitation route starting from Ca nitrate yields harder agglomerates (just different in mean size, as a function of the precipitation tempera-

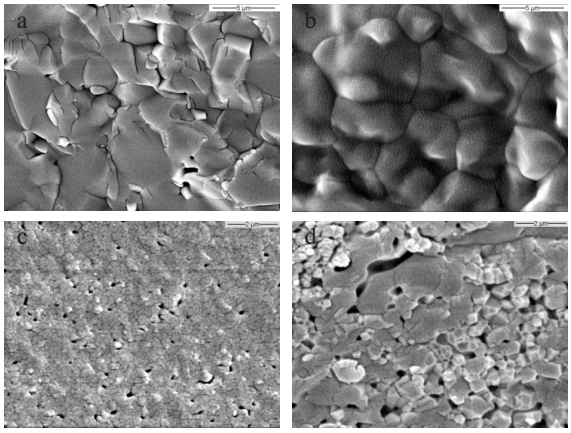

Fig. 9 SEM images of fracture surfaces of: a – HAN1 sintered at 1250°C for 1 h; b – HAN3 sintered at 1250°C for 1 h; c – HAI1 sintered at 1050°C for 3 h; d – HAN2 sintered at 1050°C for 3 h

Table 4 Sintering data of the four HA powders

Sample	Green density/ g cm^{-3} (%)*	Fired density/ g cm^{-3} (%) 1250°C*	Linear shrinkage/ %	Inflection temperature/°C	Fired density/ g cm^{-3} (%) 1050°C*
HAN1	1.68 (54)	2.90 (94)	18.2	1040	2.66 (86)
HAN2	1.54 (50)	2.75 (89)	17.7	1030	2.69 (87)
HAN3	1.58 (51)	2.86 (93)	19.5	1010	2.78 (90)
HAI1	1.62 (52)	2.80 (91)	18.3	1050	2.82 (92)

*referred to theoretical value of pure HA, d^{th}=3.08 g cm^{-3}, and to materials sintered at two different maximum sintering temperature

ture). These phenomena led to microstructural dishomogeneities characterised by more or less dense regions surrounded by large pores.

Conclusions

From the above systematic study the following conclusions can be drawn out:

- The pivotal role of the type of the preparation process on the thermal stability of HA powders as well as on their sintering behaviour and final fired microstructure has been clearly pointed out;
- Synthesis temperature affects crystallite size, shape factor, and crystallinity degree. No relevant effect of reactant concentration was evidenced. In any case, the type of precipitation route seems to be the most relevant parameter in determining HA nano-features;
- HAI1, despite of its Ca/P molar ratio slightly higher than the stoichiometric one, presents phase stability up to 1300°C, whereas all the HAN materials above 800°C yield TCP as second phase. Mg and Sr contamination does not seem to affect HA stability;
- Sintering HAI1 at 1050°C yields dense and nanostructured bodies, whereas at the same temperature all HAN powders lead to dishomogeneous microstructure, entrapping large pores probably induced by hard agglomeration.

The production of HA nano-powders from Ca nitrate route, thermally-stable up to high temperature, will allow the overall comparison between the above synthesis routes.

Acknowledgements

The Authors are greatly indebted to European Commission to having partially supported research in the framework of Integrated Project NanoKer; to Prof. E. Bemporad and Mr. D. De Felicis of University of Rome 3, Italy, for TEM analyses; Dr. E. Bauer, of ISM, CNR-Montelibretti, Rome, Italy, for the access to FTIR facilities.

References

1 S. Zhang and K. E. Gonsalves, J. Mater. Sci. Mater. Med., 8 (1997) 25.
2 J. Liu, X. Ye, H. Wang, M. Zhu, B. Wang and H. Yan, Ceram. Int., 29 (2003) 629.
3 K. Ioku, S. Yamauchi, S. Fujimori, S. Goto and M. Yoshimura, Solid State Ionics, 151 (2002) 147.
4 S. Z. C. Liou, S. Y. Chen and D. M. Liu, Biomaterials, 24 (2003) 3981.
5 S. Meejoo, W. Maneeprakorn and P. Winotai, Thermochim. Acta, 447 (2006) 115.
6 J.-K. Han, H.-Y. Song, F. Saito and B.-T. Lee, Mater. Chem. Phys., 99 (2006) 235.
7 T. J. Webster, C. Ergun, R. H. Doremus, R. W. Siegel and R. Bizios, Biomaterials, 24 (2001) 1327.
8 C. Kothapalli, M. Wei, A. Vasileiv and M. T. Shaw, Acta Mater., 52 (2004) 5655.
9 C.Puajindanetr, S. M. Best and W. Bonfield, Br. Ceram. Trans., 93 (1994) 96.
10 H. Y. Juang and M. H. Hon, Biomaterials, 17 (1995) 2059.
11 N. Kivrak and A. Cuneyt Tas, J. Am. Ceram. Soc., 81 (1998) 2245.
12 M. A. Fanovich and J. M. Porto Lopez, J. Mater. Sci. Mater. Med., 9 (1998) 53.
13 E. Landi, A. Tampieri, G. Celotti and S. Sprio, J. Eur. Ceram. Soc., 20 (2000) 2377.
14 A. Cuneyt Tas, Biomaterials, 21 (2000) 1429.
15 N. Thangamani, K. Chinnakali and F. D. Gnanam, Ceram. Int., 28 (2002) 355.
16 S. Raynaud, E. Champion, D. Bernache-Assolant and P. Thomas, Biomaterials, 23 (2002) 1065.
17 S. Raynaud, E. Champion and D. Bernache-Assolant, Biomaterials, 23 (2002) 1073.
18 N. Y. Mostafa, Mater. Chem. Phys., 94 (2005) 333.
19 L. B. Kong, J. Ma and F. Boey, J. Mater. Sci., 37 (2002) 1131.
20 A. Siddharthan, S. K. Seshadri and T. S. Sampath Kumar, J. Mater. Sci. Mater. Med., 15 (2004) 1279.
21 Y.-M. Sung, J.-C. Lee and J.-W. Yang, J. Cryst. Growth, 262 (2004) 467.
22 A. Tampieri, G. Celotti, E. Landi and M. Sandri, Key Eng. Mater., 264–268 (2004) 2051.
23 M. Kikuchi, A. Yamazaki, R. Otsuka, M. Akao and H. Aoki, J. Solid State Chem., 113 (1994) 373.
24 B. E. Yoldas, J. Am. Ceram. Soc., 65 (1982) 387.
25 P. Palmero, C. Esnouf, L. Montanaro and G. Fantozzi, J. Eur. Ceram. Soc., 25 (2005) 1565.
26 Y. X. Pang and X. Bao, J. Eur. Ceram. Soc., 23 (2003) 1697.
27 E. Bouyere, F. Gitzhofer and M. I. Boulos, J. Mater. Sci. Mater. Med., 11 (2000) 523.
28 A. Krajewski, M. Mazzocchi, P. L. Buldini, A. Ravaglioli, A. Tinti, P. Taddei and C. Fagnano, J. Mol. Struct., 744–747 (2005) 221.
29 H. Oudadesse, A. C. Derrien and M. Lefloch, J. Therm. Anal. Cal., 82 (2005) 323.
30 R. M. Wilson, J. C. Elliott, S. E. P. Dowker and R. I. Smith, Biomaterials, 25 (2004) 2205.
31 F. Apfelbaum, H. Diab, I. Mayer and J. B. D. Feather, J. Inorg. Biochem., 66 (1997) 1.
32 G. Xu, I. A. Aksay and J. T. Groves, J. Am. Chem. Soc., 123 (2001) 2196.
33 S. C. G. Leeuwenburgh, J. G. C. Wolke, J. Schoonman and J. A. Jansen, J. Biomed. Mater. Res., 66A (2003) 330.
34 S. C. G. Leeuwenburgh, J. G. C. Wolke, J. Schoonman and J. A. Jansen, Biomaterials, 25 (2004) 641.
35 P. E. Wang and T. K. Chaki, J. Mater. Sci. Mater. Med., 4 (1993) 150.
36 G. C. Koumoulidis, C. C. Trapalis and T. C. Vaimakis, J. Therm. Anal. Cal., 84 (2006) 165.

DOI: 10.1007/s10973-006-8011-6